

## Unveiling the catalytic potential of two-dimensional boron nitride in lithium–sulfur batteries

Khossossi, Nabil; Singh, Deobrat; Essaoudi, Ismail; Ahuja, Rajeev; Ainane, Abdelmajid

**DOI**

[10.1016/j.cej.2023.147518](https://doi.org/10.1016/j.cej.2023.147518)

**Publication date**

2024

**Document Version**

Final published version

**Published in**

Chemical Engineering Journal

**Citation (APA)**

Khossossi, N., Singh, D., Essaoudi, I., Ahuja, R., & Ainane, A. (2024). Unveiling the catalytic potential of two-dimensional boron nitride in lithium–sulfur batteries. *Chemical Engineering Journal*, 479, Article 147518. <https://doi.org/10.1016/j.cej.2023.147518>

**Important note**

To cite this publication, please use the final published version (if applicable). Please check the document version above.

**Copyright**

Other than for strictly personal use, it is not permitted to download, forward or distribute the text or part of it, without the consent of the author(s) and/or copyright holder(s), unless the work is under an open content license such as Creative Commons.

**Takedown policy**

Please contact us and provide details if you believe this document breaches copyrights. We will remove access to the work immediately and investigate your claim.



# Unveiling the catalytic potential of two-dimensional boron nitride in lithium–sulfur batteries

Nabil Khossossi <sup>a,\*</sup>, Deobrat Singh <sup>c</sup>, Ismail Essaoudi <sup>b</sup>, Rajeev Ahuja <sup>c,d</sup>, Abdelmajid Ainane <sup>b</sup>

<sup>a</sup> Department of Materials Science and Engineering, Faculty of Mechanical, Maritime and Materials Engineering, Delft University of Technology, Mekelweg 2, Delft, 2628 CD, The Netherlands

<sup>b</sup> Laboratory of Material Physics & Systems Modeling, Faculty of Sciences, Department of Physics, Moulay Ismail University, Meknes, Morocco

<sup>c</sup> Condensed Matter Theory Group, Materials Theory Division, Department of Physics and Astronomy, Uppsala University, Box 516, 75120 Uppsala, Sweden

<sup>d</sup> Department of Physics, Indian Institute of Technology Ropar, Rupnagar 140001, Punjab, India

## ARTICLE INFO

### Keywords:

2D o-B<sub>2</sub>N<sub>2</sub> monolayer  
Electrocatalytic properties  
Shuttle effect  
Lithium polysulfide  
Organic electrolyte  
First-principles calculations

## ABSTRACT

Lithium–sulfur (Li–S) batteries, renowned for their potential high energy density, have attracted attention due to their use of earth-abundant elements. However, a significant challenge lies in developing suitable materials for both lithium-based anodes, which are less prone to lithium dendrite formation, and sulfur-based cathodes. This obstacle has hindered their widespread commercial viability. In this study, we present a novel sulfur host material in the form of a two-dimensional semiconductor boron nitride framework, specifically the 2D orthorhombic diboron dinitride (o-B<sub>2</sub>N<sub>2</sub>). The inherent conductivity of o-B<sub>2</sub>N<sub>2</sub> mitigates the insulating nature often observed in sulfur-based electrodes. Notably, the o-B<sub>2</sub>N<sub>2</sub> surface demonstrates a high binding affinity for long-chain Li-polysulfides, leading to a significant reduction in their dissolution into the DME/DOL electrolytes. Furthermore, the preferential deposition of Li<sub>2</sub>S on the o-B<sub>2</sub>N<sub>2</sub> surface expedites the kinetics of the lithium polysulfide redox reactions. Additionally, our investigations have revealed a catalytic mechanism on the o-B<sub>2</sub>N<sub>2</sub> surface, significantly reducing the free energy barriers for various sulfur reduction reactions. Consequently, the integration of o-B<sub>2</sub>N<sub>2</sub> as a host cathode material for Li–S batteries holds great promise in suppressing the shuttle effect of lithium polysulfides and ultimately enhancing the overall battery performance. This represents a practical advancement for the application of Li–S batteries.

## 1. Introduction

The growing adoption of electric vehicles (EVs) has spurred a focused endeavor aimed at advancing rechargeable battery technologies to attain superior electrochemical capabilities, particularly characterized by high-energy density, prolonged cycle-life, and high operational temperatures [1,2]. Among the most commonly-used types on today's market is the lithium-ion battery, which is based on the so-called Li-intercalation mechanism. [3,4]. However, their operational safety and efficiency continue to raise significant concerns. Capacity degradation with aging is a principal apprehension, attributed to various mechanisms such as the formation and dissolution of the Solid-Electrolyte-Interphase (SEI) [5,6].

Li–sulfur batteries (LiSBs) constitute an outstanding alternative for electrochemical energy storage systems and have attracted considerable attention due to their low price and increased theoretical capacity of about 1675 mAh.g<sup>-1</sup> and high energy density of about

2600 W.h.kg<sup>-1</sup> [7–13]. Diverging from conventional rechargeable batteries featuring intercalated lithium compound cathodes and graphene-based anodes, Li–S batteries operate through the reversible redox-reaction of Sulfur↔Li<sub>2</sub>S at the cathode, involving numerous intermediate Li<sub>2</sub>S<sub>n</sub> species (n = 2, 4, 6, 8). The incorporation of an organic binary solvent into the electrolyte composition facilitates the dissolution of the insulating Li-polysulfides Li<sub>2</sub>S<sub>n</sub>, thereby enhancing S-element utilization and elevating energy density. Notwithstanding, the dissolution and scattering of Li<sub>2</sub>S<sub>n</sub> within the electrolyte give rise to the depletion of the S-containing cathode, alongside the phenomenon of the Li<sub>2</sub>S<sub>n</sub> shuttle effect, leading to a rapid reduction in specific capacity, energy density, and coulombic efficiency [2,14,15,15].

Considerable efforts have been directed towards mitigating the insulating and dissolution challenges associated with sulfur and lithium polysulfides (LiPSs). In pursuit of advanced cathode materials, carbon-based substances have emerged for their exceptional electrical conductivity and robust mechanical properties, rendering them suitable

\* Corresponding author.

E-mail addresses: [n.khossossi@edu.umi.ac.ma](mailto:n.khossossi@edu.umi.ac.ma) (N. Khossossi), [a.ainane@fs-umi.ac.ma](mailto:a.ainane@fs-umi.ac.ma) (A. Ainane).

<https://doi.org/10.1016/j.cej.2023.147518>

Received 18 August 2023; Received in revised form 31 October 2023; Accepted 17 November 2023

Available online 19 November 2023

1385-8947/© 2023 The Author(s). Published by Elsevier B.V. This is an open access article under the CC BY license (<http://creativecommons.org/licenses/by/4.0/>).

candidates as hosts for sulfur cathodes in lithium–sulfur batteries [16–20]. Despite this, the weak interaction of non-polar carbons with polar LiPSs barely prevents the dissolution of  $\text{Li}_2\text{S}_n$  intermediates in the electrolyte as well as the shuttling between the cathode and the Li-anode [21,22].

Nanostructured polar inorganic materials, including transition metal-based metal oxides and sulfides, have demonstrated robust binding capabilities, effectively sequestering LiPSs [12,22–25]. However, several of these inorganic hosts exhibit notably poor electrical conductivity in comparison to conventional carbon-based host cathodes, resulting in compromised rate performance and limited specific capacity. Additionally, porous carbon and metal-based van der Waals (vdW) heterostructures have been shown to overcome shuttle effects and enhance the exceptional electrochemical properties of LiSBs [26–30]. Furthermore, a broad team of researchers remains engaged in a continuous endeavor to conceive novel and intriguing materials, serving as economically viable hosts for sulfur incorporation within conventionally established LiSBs.

In recent years, substantial attention has been directed towards the advancement of host cathode materials for LiSBs, resulting in remarkable strides in the field. Within these versatile prospects, two-dimensional (2D) materials have emerged as a particularly promising alternative, leveraging their distinct physical and chemical properties relative to their bulk counterparts, which can provide great electro-chemical features [4,13,31,32]. Within this context, an extensive spectrum of 2D materials, including  $\beta_{12}$ -borophene [33],  $\alpha$ - and  $\beta$ -phase phosphorene [34–36], hexagonal BN [37], graphene-supported BN monolayers [38], transition metal sulfides, and carbonitrides [39–43], have been systematically investigated through the density functional theory and/or experimental approaches. This comprehensive exploration has been undertaken with the aim of devising a host cathode material that can engender enhanced high-performance Li–S batteries. Notwithstanding these advancements, a substantial number of the identified 2D materials grapple with various limitations, encompassing compromised stability, feeble LiPSs adsorption impeding the mitigation of the shuttle effect, inadequate charge and discharge efficiency, poor electrical conductivity, inherent instability, and/or cost-intensive manufacturing processes. Consequently, a pressing ruling within the LiSB domain is the continued research and development of an improved 2D sulfur host material endowed with elevated electro-chemical characteristics, to meet the exigent requirements of enhanced Li–S battery technologies.

Although graphene-like boron nitride (h-BN) has gained substantial attention across considerable applications due to its wide indirect band-gap (6 eV) [44,45], its non-performance as a host cathode anchoring material in LiSBs can primarily be attributed to its substantial band-gap, a characteristic incompatible with the requisite enhanced electronic conductivity of cathode hosts [16,46,47]. Additionally, the weak interaction between Li-polysulfides and the h-BN surface has curtailed its suitability for LiSBs applications [37]. Addressing this, Demirci et al. (2020) introduced a novel orthorhombic structure (o- $\text{B}_2\text{N}_2$ ) of graphene-like boron nitride, derived from density functional theory (DFT) calculations [48]. In-depth investigations into dynamic and mechanical stability have confirmed the dynamical and mechanical robustness of the o- $\text{B}_2\text{N}_2$  monolayer. Ab-initio molecular dynamics simulations further revealed the monolayer's structural integrity up to 1000 K for 10 ps. The newly proposed o- $\text{B}_2\text{N}_2$ , characterized as a semiconductor with a direct narrow bandgap of 0.64 eV, unveils a plethora of potential applications in the realm of energy-related systems. In the current study, employing density functional theory calculations, we unveil that the 2D orthorhombic boron nitride allotrope fulfills the requirement of an optimal S-host cathode for Li–S batteries. The enhanced electronic conductivity exhibited by o- $\text{B}_2\text{N}_2$  relative to its h-BN counterpart addresses the insulating tendencies inherent to most S-based cathodes. The robust binding affinity of the o- $\text{B}_2\text{N}_2$  monolayer towards  $\text{Li}_2\text{S}_n$  ( $n = 8, 6, 4, 2,$  and  $1$ ) polysulfides effectively curtails the

dissolution of Li-polysulfides into the organic electrolytes, namely 1,2-dimethoxyethane (DME) and 1,3-dioxolane (DOL). Furthermore, the uniform adsorption configuration of  $\text{Li}_2\text{S}$  on the o- $\text{B}_2\text{N}_2$  monolayer, ensuring electrical contact, not only enhances the versatility of the active materials but also promotes rapid conversion kinetics of  $\text{Li}_2\text{S}$  to  $\text{Li}_2\text{S}_n$  ( $n = 2, 4, 6,$  and  $8$ ) polysulfides. These insightful findings are poised to stimulate forthcoming experimental explorations within the realm of advanced Li–S batteries, leveraging the unique characteristics of this novel 2D orthorhombic boron nitride allotrope.

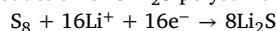
## 2. Methods and computational details

### Density functional theory

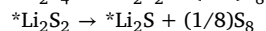
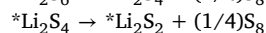
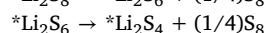
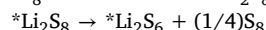
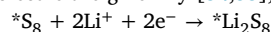
Through our study, we performed first-principles calculations within the framework of Density Functional Theory (DFT) as part of the Vienna Ab Initio Simulation Package (VASP) [49]. The generalized gradient approximation in the form of Perdew Burke Ernzerhof (PBE) functional [50] was adopted self-consistently through the approach of the Projector Augmented Wave (PAW) by Kohn–Sham electron wave functions expanded with an energy cutoff of 600 eV and the convergence criteria during the structural optimizations were set to  $10^{-6}$  eV and  $10^{-3}$  eV/Å for energy and force, respectively. To mitigate interactions between stacked layers and periodic images, a vacuum layer of 25 Å was introduced along the  $z$ -direction throughout all computations. To ensure the rigor and accuracy of our results, it was crucial to select an appropriate k-point grid for our calculations. This selection was based on a convergence test that probed the relationship between total energy and various K-points. Our analysis indicated that a Monkhorst Pack K-point grid of approximately  $8 \times 16 \times 1$  in the reciprocal space provided the most consistent results during geometrical optimizations [51]. Additionally, we employed the Bader charge algorithm to evaluate the charge transfer between atoms [52].

### Gibbs free energy of sulfur reduction reaction (SRR)

Generally, the sulfur reduction reaction of an  $\text{S}_8$ -molecule through the discharging process of LiSBs is a 16-electron process along with the production of 8- $\text{Li}_2\text{S}$  polysulfides [53].



The rudimentary stages involved in the formation of one  $\text{Li}_2\text{S}$  molecule are given by [54,55];



Wherein (\*) represents an active site on the material surface.

For each stage of the SRR, the reaction Gibbs free energy is given through the following equations:

$$\Delta G = \Delta E + \Delta E_{ZPE} - T\Delta S, \quad (1)$$

$\Delta E$  is the differential adsorption energy calculated for intermediate molecules adsorbed on the material's surface,  $\Delta E_{ZPE}$  is the difference in zero-point energies correction, and  $T\Delta S$  is the variation in entropy from the adsorbed to the gas phase computed at 298.15 K.

The variation in Gibbs free energy at every electrochemical stage of the SRR can be derived by the given equations;

$$\Delta G_1 = (E_{*\text{Li}_2\text{S}_8} + E_{ZPE(*\text{Li}_2\text{S}_8)} - T S_{*\text{Li}_2\text{S}_8}) + (E_{*\text{S}_8} + E_{ZPE(*\text{S}_8)} - T S_{*\text{S}_8}) - 2.(E_{\text{Li}} + E_{ZPE(\text{Li})} - T S_{\text{Li}}),$$

$$\Delta G_2 = (E_{*\text{Li}_2\text{S}_6} + E_{ZPE(*\text{Li}_2\text{S}_6)} - T S_{*\text{Li}_2\text{S}_6}) + (1/4).(E_{*\text{S}_8} + E_{ZPE(*\text{S}_8)} - T S_{*\text{S}_8}) - (E_{*\text{Li}_2\text{S}_8} + E_{ZPE(*\text{Li}_2\text{S}_8)} - T S_{*\text{Li}_2\text{S}_8}),$$

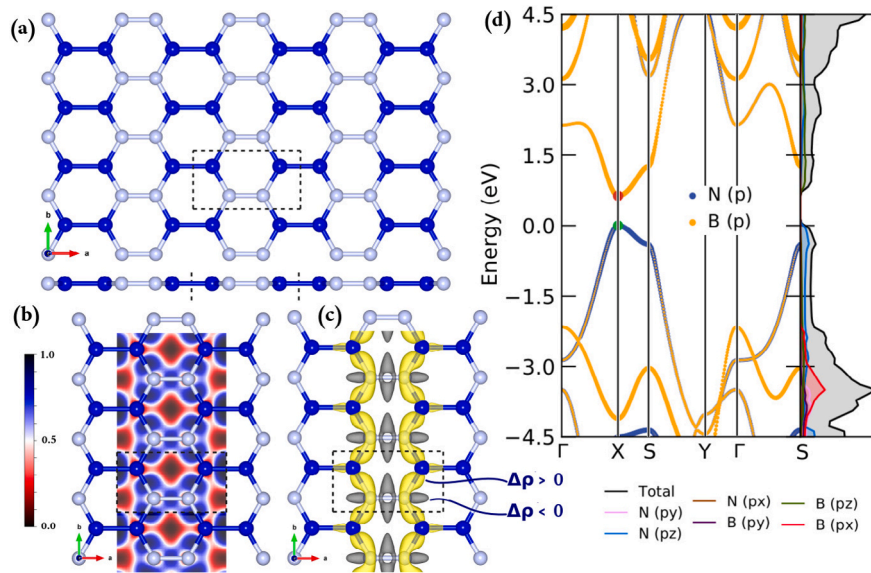


**Fig. 1.** (a) Top and side views of a free-standing orthorhombic diboron dinitride o-B<sub>2</sub>N<sub>2</sub> monolayer. The dashed lines show the unit cell. (b) The electron localization function (ELF) of the o-B<sub>2</sub>N<sub>2</sub> with the red (blue) zones indicating low (high) localized electrons. (c) The difference charge density of the o-B<sub>2</sub>N<sub>2</sub> surface with the yellow and gray refer to electron accumulation and depletion, respectively. (d) The projected band structure of the o-B<sub>2</sub>N<sub>2</sub> monolayer through GGA-PBE calculation with corresponding total/partial density of state.

$$\begin{aligned} \Delta G_3 &= (E_{Li_2S_4} + E_{ZPE(*Li_2S_4)} - TS_{*Li_2S_4}) \\ &+ (1/4)(E_{*S_8} + E_{ZPE(*S_8)} - TS_{*S_8}) \\ &- (E_{*Li_2S_6} + E_{ZPE(*Li_2S_6)} - TS_{*Li_2S_6}), \\ \Delta G_4 &= (E_{Li_2S_2} + E_{ZPE(*Li_2S_2)} - TS_{*Li_2S_2}) \\ &+ (1/4)(E_{*S_8} + E_{ZPE(*S_8)} - TS_{*S_8}) \\ &- (E_{*Li_2S_4} + E_{ZPE(*Li_2S_4)} - TS_{*Li_2S_4}), \\ \Delta G_5 &= (E_{Li_2S} + E_{ZPE(*Li_2S)} - TS_{*Li_2S}) \\ &+ (1/8)(E_{*S_8} + E_{ZPE(*S_8)} - TS_{*S_8}) \\ &- (E_{*Li_2S_2} + E_{ZPE(*Li_2S_2)} - TS_{*Li_2S_2}), \end{aligned}$$

### 3. Results and discussion

The initial investigation encompassed the examination of structural and electronic properties pertaining to the free-standing monolayer configuration of 2D o-B<sub>2</sub>N<sub>2</sub>. The top and side views of the fully relaxed o-B<sub>2</sub>N<sub>2</sub> monolayer are depicted in Fig. 1(a,b) with a dashed line crystallizing in a graphene-like 2D structure with a sequence of B-B and N-N bonds interconnected to each other and collectively formulate an orthorhombic unit-cell under the D<sub>2h</sub> symmetry. The optimized lattice parameters are about a = 4.570 Å and b = 2.496 Å, and B-B, B-N, and N-N bond lengths are observed to be 1.701, 1.438, and 1.438 Å, correspondingly. These findings align cohesively with prior reports in the literature [48, 56]. Further insights into the chemical bonding characteristics of the o-B<sub>2</sub>N<sub>2</sub> monolayer were garnered through the computation and display of the electron localization function (ELF) and the 2D projected difference charge density, as depicted in Fig. 1(c,d). This analysis aimed to elucidate the intricate nature of chemical bonding within the o-B<sub>2</sub>N<sub>2</sub> monolayer. The examination reveals that both the B-B and B-N bonds are characterized by high localized electrons densities in contrast to the N-N bond, which exhibits notably diminished localized electrons. This observation signifies the robust covalent bonding character of both B-B and B-N bonds, in juxtaposition to the comparatively weaker covalent bonding nature of the N-N bond. Evidently, as illustrated in Fig. 1(c), the charge distribution predominantly involves the transfer of charge from B atoms to N atoms, yielding a charge transfer of approximately 0.907 |e| per atom as determined by Bader charge analysis.

The projected electronic band-structure with the projected density-of-states is shown in Fig. 1(d) using the PBE functional. The o-B<sub>2</sub>N<sub>2</sub> monolayer shows a semiconductor nature with a direct bandgap of about 0.647 eV much smaller than the h-BN monolayer (4.446 eV), where the VBM and CBM are located at X-point. which is very significant for enhancing the rate performance as well as the specific capacity of Li-S batteries. The rationale underlying the band gap narrowing can be explained by the total and partial density of state as illustrated in Fig. 1(d). It is obvious that the e-states around the Fermi level mainly derive from the pz-orbitals of both B- and N-atoms. Compared to other semiconducting boron nitride allotrope materials, the small band gap of the o-B<sub>2</sub>N<sub>2</sub> monolayer proves to be a very suitable sulfur host material for Li-S batteries.

Furthermore, the sulfur-atoms typically occur in the electrode as an orthorhombic structure with the chemical formula α-S<sub>8</sub>, being the more stable molecular allotrope at ambient temperature. The primary reduced chemical components throughout the discharge process are Li<sub>2</sub>S<sub>n</sub> with n = 8, 6, 4, and 2, respectively, and Li<sub>2</sub>S as the final component of S-reduction. Fig. 2(a,b) shows the fully optimized molecular structures of S<sub>8</sub>, polysulfides Li Li<sub>2</sub>S<sub>n</sub> (n = 8, 6, 4, 2, and 1), and the organic electrolytes 1,2-dimethoxyethane (DME) and 1,3-dioxolane (DOL). All the free-standing molecular structures are optimized in 3D shape instead of linear-chains, in good agreement with the previous reports. The Fig. 2(c) show the S-S and Li-S bond lengths, once can noticed that as the number of S-atom increase, the Li-S bond length increase from Li<sub>2</sub>S to Li<sub>2</sub>S<sub>6</sub> and d<sub>S-S</sub> decrease, indicating the high interaction between Sulfur atoms. Consequently, it can be concluded that the long-chain Li<sub>2</sub>S<sub>n</sub> (n = 8, 6, and 4) molecules are more conveniently ionized into Li<sup>+</sup> and polysulfide anions, leading to the so-called shuttling effect.

A large super-cell of about 3 × 4 × 1 of 2D o-B<sub>2</sub>N<sub>2</sub> monolayer was adopted as the anchoring material to study the binding strength of S<sub>8</sub> and Li<sub>2</sub>S<sub>n</sub> (n = 8, 6, 4, 2, and 1) polysulfides. In the process of searching for the most stable binding configurations, we have fully optimized various orientations of S<sub>8</sub> and LPSs clusters at possible binding sites on the o-B<sub>2</sub>N<sub>2</sub> surface. The principle, which consists of recognizing the privileged binding site energetically, is derived according to the binding strength formula given above by means of vdW and without vdW correction:

$$E_b = E_{B_2N_2} + E_S - E_{S@B_2N_2} \quad (S = S_8/Li_2S_n) \quad (2)$$



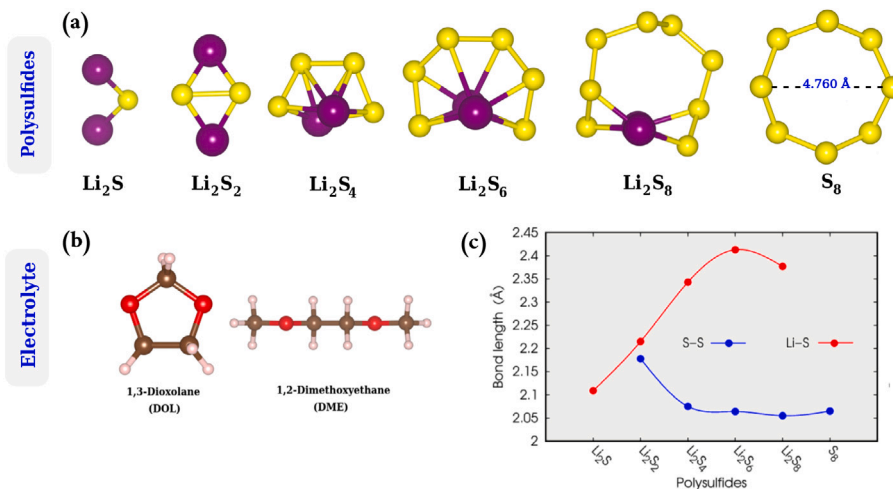


Fig. 2. (a) The optimized molecular structures of  $\text{S}_8$  and  $\text{Li}_2\text{S}_n$  ( $n = 8, 6, 4, 2, 1$ ). (b) Optimized structures of organic electrolyte 1,2-dimethoxyethane (DME) and 1,3-dioxolane (DOL). (c) The optimized bond lengths for S-S and Li-S for different polysulfides.

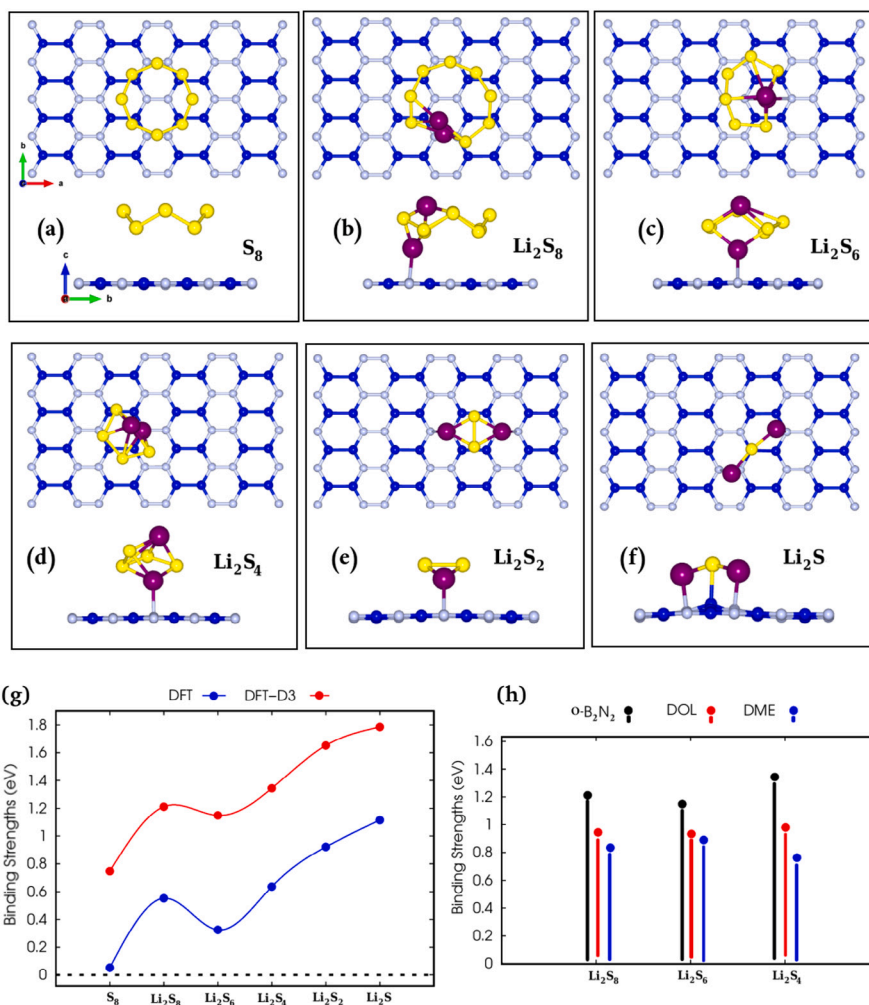


Fig. 3. The top and side views of the fully optimized structures of (a)  $\text{S}_8$ , (b)  $\text{Li}_2\text{S}_8$ , (c)  $\text{Li}_2\text{S}_6$ , (d)  $\text{Li}_2\text{S}_4$ , (e)  $\text{Li}_2\text{S}_2$  (f)  $\text{Li}_2\text{S}$  clusters adsorbed on the most stable site of  $o\text{-B}_2\text{N}_2$  monolayer through DFT-D3 correction. (g) Computed binding strengths of  $\text{S}_8/\text{Li}_2\text{S}_n$  clusters on the  $o\text{-B}_2\text{N}_2$  monolayer through DFT and DFT-D3 correction. (h) Comparison of the binding strengths of  $\text{Li}_2\text{S}_n$  ( $n=8,6,4$ ) clusters between the  $o\text{-B}_2\text{N}_2$  monolayer and organic electrolytes, mainly, 1,3-dioxolane (DOL) and 1,2-dimethoxyethane (DME).

**Table 1**

Computed binding strength of  $S_8/Li_2S_n$  molecules on  $o-B_2N_2$  surface using DFT and DFT-D3, shortest binding height, charge transfer  $\Delta Q$  ( $|e|$ )<sup>a</sup> between  $S_8/Li_2S_n$  and the anchoring material.

$S_8/Li_2S_n$ molecules	$E_b^{DFT}$ (eV)	$E_b^{DFT-D3}$ (eV)	$\Delta Q$ ( $ e $ )	h (Å)
$S_8$	0.053	0.747	-0.003	3.325
$Li_2S_8$	0.552	1.212	0.238	2.183
$Li_2S_6$	0.325	1.149	0.317	2.046
$Li_2S_4$	0.636	1.343	0.471	1.994
$Li_2S_2$	0.922	1.652	0.515	1.893
$Li_2S$	1.115	1.786	0.753	1.554

<sup>a</sup>  $\Delta Q > 0$  reveals the electrons transfer from  $S_8/Li_2S_n$  to the  $o-B_2N_2$  surface.

Wherein  $E_{Total}$  and  $E_{B_2N_2}$  refers to the total energies of  $o-B_2N_2$  surface after and before the adsorption of  $S_8/Li_2S_n$  molecules, respectively,  $E_S$  the average total energy of  $S_8/Li_2S_n$  in bulk reference state with a lattice constant of 25 Å. Typically, the use of the vdW-correction significantly affects the binding strengths; therefore, the energies have been evaluated with and without the vdW-correction. [4,57]. In this context, the more the binding strength is positive, the more the binding configuration is more stable, indicating an exothermic reaction and the scattering distribution of the adsorbed  $S_8/Li_2S_n$  molecules instead of their clustering. Therefore, avoiding the issues arising from the formation of metal-dendrites or metal-clusters during the charge/discharge process. Within the binding sites and orientations explored, the most stable configurations with the lowest binding strength are illustrated in Fig. 3(a–f). The binding strengths of  $S_8$  and  $Li_2S_n$  molecules on the  $o-B_2N_2$  surface are outlined in Table 1. The Fig. 3(a), it can be clearly noticed that the  $S_8$  cluster adsorbed right above the  $B_2N_4$ -hexagon rings and parallel to the  $o-B_2N_2$  surface with the shortest binding height of about 3.325 Å, very larger compared to the N–B, B–B, and N–N bond lengths. The binding energy of a  $S_8$ -molecule adsorbed on  $o-B_2N_2$  monolayer is 0.747 eV through the vdW-correction, which indicate that the binding is dominated by weak vdW interaction with a very negligible charge transfer of about  $-0.003 |e|$  transferred from the  $o-B_2N_2$  monolayer to the  $S_8$  cluster.

Additionally, it is worth highlighting that the adsorption of  $S_8$  cluster displays no structural deformation of the cluster and anchoring material, while the high-order  $Li_2S_n$  (with  $n = 8, 6, 4$ ) polysulfides adsorbed on the  $o-B_2N_2$  monolayer shows a very slight structural deformation with respect to the isolated polysulfide molecules as displayed in Fig. 3(b,c,d) with high-affinity characteristics. High-order lithium polysulfides exhibit a propensity to align parallel to the  $o-B_2N_2$  substrate, predominantly through the formation of a Li–B bond. This orientation and bond formation resonate with the Li bond chemistry observed in various systems [58–60]. Such interactions suggest a direct chemical bonding between the soluble  $Li_2S_n$  intermediates and the  $o-B_2N_2$  anchoring framework.

As shown in Fig. 3(g) and Table 1, the binding strengths of the high-order  $Li_2S_n$  (with  $n = 8, 6, 4$ ) on the  $o-B_2N_2$  surface are approximately 1.212, 1.149, and 1.343 eV, respectively, ranging in the desirable window of 0.8–2.0 eV, which can be regarded as an important factor in assessing the applicability of anchoring materials for Li–S batteries. [61] According to our findings, the weakening of the Li–S bond caused by the dissolution of  $Li_2S_n$  molecules within the organic electrolyte could be significantly reduced and prevented. Thereby indicating the 2D  $o-B_2N_2$  monolayer as a prospective anchoring material with a moderate binding strength of  $Li_2S_n$  clusters.

Within the landscape of Li–S batteries, both the electrolyte and associated Li salts critically influence the cell's overall performance. To comprehensively understand the anchoring capabilities of the  $o-B_2N_2$  to discharge  $S_8/Li_2S_n$  products, it is essential to identify the electrolytes' intrinsic role, particularly 1,2-dimethoxyethane (DME) and 1,3-dioxolane (DOL), which we adopted in our study. These were

selected due to their inherent advantages that underpin efficient battery operation. Specifically, DME and DOL offer a balance of low polysulfide concentrations and superior ionic conductivity, directly influencing the battery's kinetics and rate capabilities [62–64]. The binding strengths of high-order  $Li_2S_n$  ( $n = 8, 6,$  and  $4$ ) clusters on selected standard organic electrolytes, mainly, 1,3-dioxolane (DOL) and 1,2-dimethoxyethane (DME), were derived based on the equation:

$$E_b = E_{electrolyte} + E_S - E_{S@electrolyte} \quad (S = S_8/Li_2S_n) \quad (3)$$

Where  $E_{Total}$  and  $E_{electrolyte}$  represents the total energies of organic electrolytes after and before the adsorption of  $Li_2S_n$  ( $n = 8, 6,$  and  $4$ ) molecules, respectively. In order to rationalize, we initially consider the case of one  $Li_2S_n$  cluster binding with one organic electrolyte molecule. The Figure S1 in ESI, depict the full relaxed  $Li_2S_n@(DME/DOL)$ -electrolyte systems. One can clearly notice that the binding of the  $Li_2S_n$  clusters on (DME/DOL)-electrolyte are primarily driven by lithium-atoms of the  $Li_2S_n$  clusters with the O-atoms of the organic solvent DME/DOL. As shown in Figure S1 (ESI), the computed binding strengths of the high-order  $Li_2S_n$  ( $n = 8, 6,$  and  $4$ ) molecules with the (DOL)-electrolyte are approximately 0.945 eV, 0.933 eV, and 0.980 eV and with (DME)-electrolyte of about 0.835 eV, 0.892 eV, and 0.762 eV. Which are significantly lower than the calculated binding strengths of  $Li_2S_n$  polysulfides adsorbed on  $o-B_2N_2$  surface, as shown in Fig. 3(h), confirming the tendency of  $Li_2S_n$  to be anchored on the  $o-B_2N_2$  surface instead of being dissolved in the organic-electrolyte.

Therefore, to simulate the effects of solvent on the electrolyte solvation, only the  $Li_2S_6$  cluster on the  $o-B_2N_2$  anchoring material upon the presence of the (DME/DOL)-solvent electrolytes were considered as a model to calculate the binding strengths. Owing to the interactions between the Li-ions of the  $Li_2S_n$  and the O-atoms of the DME/DOL-electrolyte, Only two DME/DOL solvent are able to be adsorbed and coordinated with one  $Li_2S_6$  cluster as presented in Fig. 4(a,b). One can notice clearly that the addition of first and second DME/DOL solvent slightly decrease the binding strengths of the  $Li_2S_6$  on  $o-B_2N_2$  surface. Furthermore, the adsorption of the DME/DOL solvent on the  $o-B_2N_2$  surface were computed as shown in Figure S2 (ESI), as a means of evaluating the binding strengths of  $S_8/Li_2S_n$  and (DME/DOL)- electrolyte solvent separately on the  $o-B_2N_2$  surface. The binding strengths of both DOL and DME organic solvent on the  $o-B_2N_2$  surface was estimated to be 0.502 and 0.473 eV, respectively. However, these binding strengths are considerably lower compared to the ones for  $S_8/Li_2S_n$  on the  $o-B_2N_2$  monolayer which leads to the weakened interaction with the B-atoms in the  $o-B_2N_2$  monolayer. Consequently, one can expect that the  $o-B_2N_2$  monolayer will efficiently eliminate the shuttle effect caused by the migration of soluble  $Li_2S_n$  lithium polysulfides to the Li-anode.

For the low-order  $Li_2S_2$  and  $Li_2S$  clusters, one can notice that both Li-atoms are located on top of the N-atoms, while the S-atom is bonded to the B-atom of the  $o-B_2N_2$  monolayer. Both the insoluble  $Li_2S_2$  and  $Li_2S$  clusters possess a high binding strength towards the  $o-B_2N_2$  monolayer, and significant structural distortion (3(e,f)) with a buckling parameter of about 0.137 Å and 0.578 Å, respectively. For instance, the Li–S bond-length of the  $Li_2S$  cluster after adsorption on  $o-B_2N_2$  monolayer, increased by 0.473 Å and the Li–Li angle decreased by roughly 31.052°. The B–S between the  $o-B_2N_2$  and  $Li_2S_2/Li_2S$  clusters possesses the smallest bond lengths of about 2.291/2.006 Å within the  $Li_2S_n$  clusters, which leads to the high binding strengths of 1.652/1.786 eV.

Furthermore, given the advantage of uniform  $Li_2S$  deposition to minimize the cell-resistance of the anchoring material, we have explored several binding configurations of the  $Li_2S$  cluster on the  $o-B_2N_2$  host. We started by placing two  $Li_2S$  clusters upon the ( $4 \times 5$ )-supercell of host material by using four different configurations. As a result of full optimization, it is noticed that the two  $Li_2S$  clusters tend to form a clustering network instead of forming a separate  $Li_2S$  cluster on the  $o-B_2N_2$  monolayer, as can be seen in Fig. 5(a). As the number of  $Li_2S$  clusters increases, the  $Li_2S$  clusters show a tendency to form a chain on

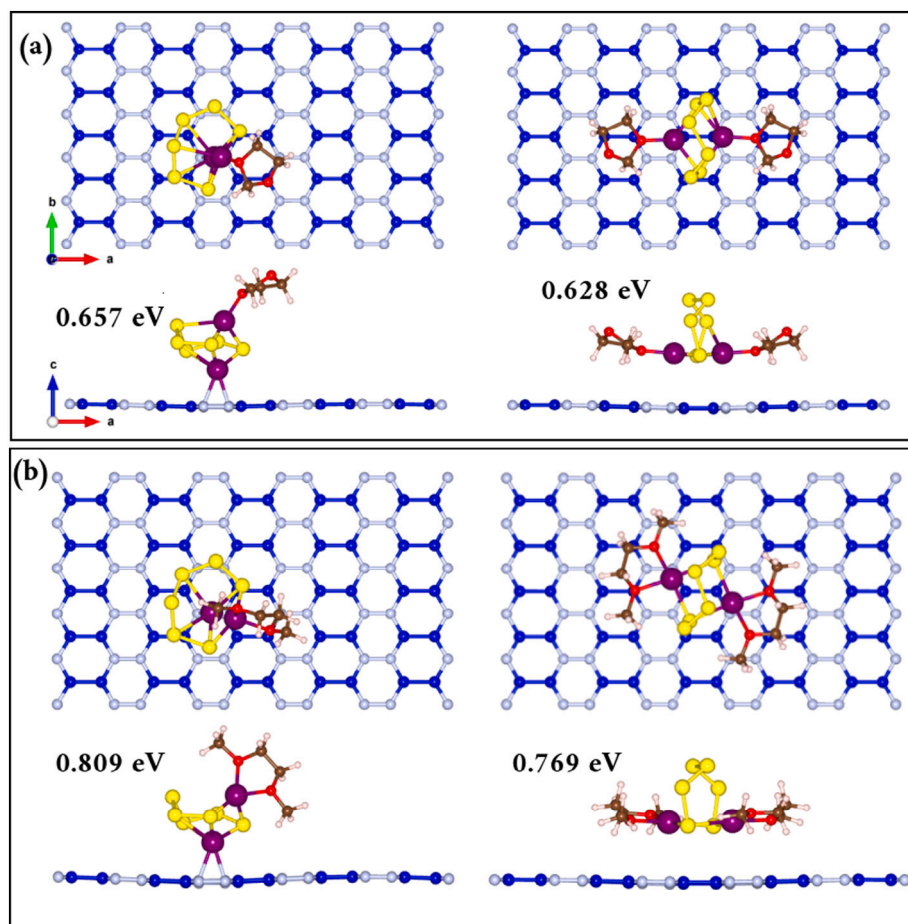


Fig. 4. The top and side views of fully optimized structures of (a) DOL molecules and (b) DME molecules decorated to the  $\text{Li}_2\text{S}_6$  molecule adsorbed on the  $\text{o-B}_2\text{N}_2$  anchoring material, with corresponding binding strengths.

the  $\text{o-B}_2\text{N}_2$  surface, as illustrated in Fig. 5(b) with a relative energy of approximately 0.182 eV. Consistent  $\text{Li}_2\text{S}$  cluster diffusion leads the insoluble  $\text{Li}_2\text{S}$  clusters to electrical contact with the host material surface, which enhances the suitability of the  $\text{o-B}_2\text{N}_2$  monolayer as well as the transformation of  $\text{Li}_2\text{S}$  and other lithium polysulfides [65]. As a result, the lithium polysulfide redox process has a fast kinetics diffusion. The arbitrary adsorption of  $\text{Li}_2\text{S}$  cluster is leading to the loss of contact with  $\text{o-B}_2\text{N}_2$  surface, drastically reducing the functionality and efficiency of Li-S batteries. In this context, the oxidation capacity of the 2D  $\text{o-B}_2\text{N}_2$  anchoring material has been investigated within the decomposition process by means of a climbing image nudged elastic band approach (CI-NEB) [13,66–68]. The computed decomposition energy profile of the  $\text{Li}_2\text{S}$  cluster on the  $\text{o-B}_2\text{N}_2$  surface is estimated to be 0.837 eV, significantly smaller compared to that of the graphene monolayer (1.81 eV), [68] yielding a rapid kinetic of the de-lithiation process.

Additionally, a more detailed understanding of the binding process and the chemical bond formation, the electronic behavior after the adsorption of  $\text{S}_8/\text{Li}_2\text{S}_n$  products was surveyed through the computation of the total and partial density of state projected on the S/Li-atom of  $\text{S}_8/\text{Li}_2\text{S}_n$  and their nearest neighboring B/N-atoms, as presented in Fig. 6. In spite of the fact that the  $\text{o-B}_2\text{N}_2$  monolayer exhibits a semiconductor with a bandgap of about 0.647 eV, it is clearly indicated that the band gaps of all the adsorption systems are reduced with an intense electronic state near to Fermi-level, which promotes electrons conduction and contributes electrons to the redox process of the adsorbed lithium polysulfides. According to the electrical conductivity given by the equation [36]:

$$\sigma \approx \exp(-\Delta E/K_b T) \quad (4)$$

Where  $\Delta E$  refers to the band gap of the system,  $K_b$  refers to the Boltzmann constant. It is expected that the reduced band gap after the adsorption of  $\text{Li}_2\text{S}_n$  products will improve the electrical conductivity of the  $\text{o-B}_2\text{N}_2$  host material through the lithiation process, which will considerably boost the efficiency of Li-S batteries.

The interaction process can be displayed by the charge density difference of  $\text{Li}_2\text{S}_n$  clusters adsorbed on  $\text{o-B}_2\text{N}_2$  monolayer by means of the formula below:

$$\Delta\rho = \rho_{S@B_2N_2} - \rho_{B_2N_2} - \rho_S \quad (S = \text{Li}_2\text{S}_n) \quad (5)$$

Where  $\rho_{B_2N_2}$  and  $\rho_{S@B_2N_2}$  denote the electron charge density of  $\text{o-B}_2\text{N}_2$  and  $\text{Li}_2\text{S}_n@B_2N_2$  systems, respectively, and  $\rho_S$  denotes the electron charge density of isolated  $\text{Li}_2\text{S}_n$  clusters by keeping the same structural parameters without any further structural relaxation. The Fig. 7(a–e) illustrates the accumulation and depletion of charges for the different systems represented as 3D isosurface distributed charge density plots. One can clearly notice that a strong charge redistribution occurs between the  $\text{Li}_2\text{S}_n$  clusters and the  $\text{o-B}_2\text{N}_2$  surface. It can be seen that charge transfer takes place via two pathways: the first via the Li-S bond while the second via the B-S bond in the case of  $\text{Li}_2\text{S}_n$  ( $n=1,2$ ). A further charge accumulation can be clearly seen in the zone adjacent to the B-atom and Li-ions. With the decrease in sulfur concentration ( $\text{Li}_2\text{S}_8 \rightarrow \text{Li}_2\text{S}$ ), the amount of charge transfer typically rises, which is in line with the binding strength tendency as summarized in Table 1.

Next, with the purpose of an in-depth understanding of the SRR performance of the host cathode  $\text{o-B}_2\text{N}_2$  material in the LiSBs discharging process, the global reaction through the reversible formation of  $\text{Li}_2\text{S}$  from  $\text{S}_8$  and Li-bulk [69] were investigated and plotted in Fig. 8. The first stage of the discharge process involves the double



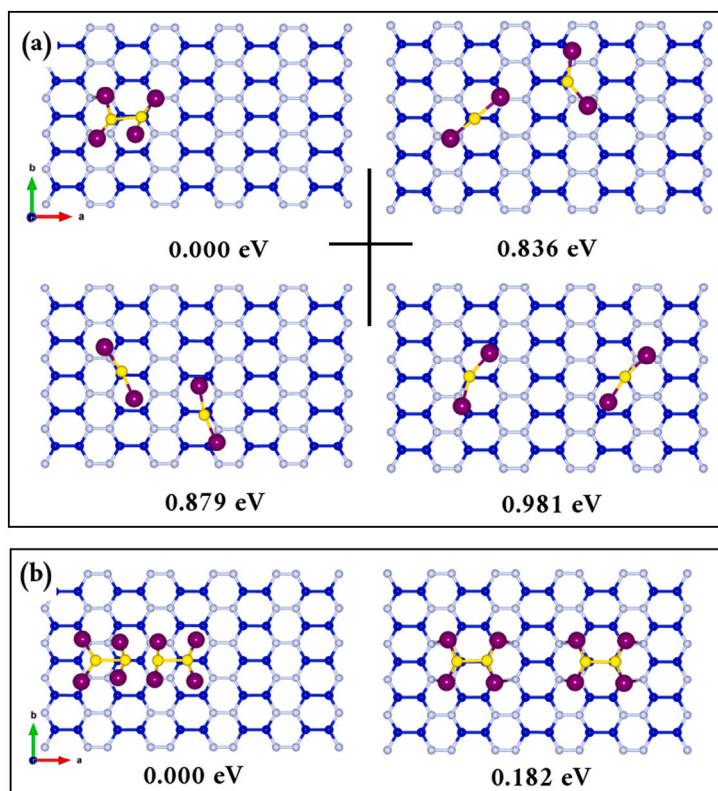


Fig. 5. Top views of fully optimized structures of two (a)  $\text{Li}_2\text{S}$  clusters and four (b)  $\text{Li}_2\text{S}$  cluster adsorbed on the  $\text{o-B}_2\text{N}_2$  surface, with corresponding relative energies.

reduction of  $\text{S}_8$ -molecule together with  $2\text{Li}^+$  to form the long-chain  $\text{Li}_2\text{S}_8$  polysulfide, after which the  $\text{Li}_2\text{S}_8$  undergoes a new reduction and disproportionately with the step-wise formation of the three intermediate lithium-polysulfides ( $\text{Li}_2\text{S}_x$  with  $x = 6, 4,$  and  $2$ ), ultimately driving to the formation of the end-product  $\text{Li}_2\text{S}$  polysulfide. It can be clearly noticed that, following the spontaneous exothermic reaction from  $\text{S}_8$  to  $\text{Li}_2\text{S}_8$  with a Gibbs free-energy of about  $-3.098$  eV, the next four reduction stages from  $\text{Li}_2\text{S}_6$  to  $\text{Li}_2\text{S}$  are endothermic ( $\Delta G > 0$ ). On the overall discharge process, the reduction stage from  $\text{Li}_2\text{S}_4$  to  $\text{Li}_2\text{S}_2$  serves as the rate-limiting stage with a positive Gibbs free-energy  $\Delta G_4 = 0.513$  eV. For the purpose of comparison, the estimated Gibbs free-energy in this work is small when compared to those obtained in the case of N-doped graphene ( $\Delta G = 0.88$  eV), single cobalt and vanadium atom on nitrogen doped graphene ( $0.72$  and  $0.84$  eV, respectively) [54,70] which indicates that the reduction of sulfur is thermodynamically more favorable on a 2D  $\text{o-B}_2\text{N}_2$  monolayer and that can significantly reduce the free-energy barrier of the sulfur reduction reaction during the discharging process and hence enhance the electrochemical features of LiSBs.

In summary, the two-dimensional orthorhombic  $\text{o-B}_2\text{N}_2$  emerges as a promising sulfur host material for Li-S batteries, endowed with a plethora of potential advantages. While its theoretical attributes hold promise, it is paramount to recognize the challenges it presents in terms of experimental realization, given that it has only been predicted theoretically and remains unsynthesized. Nevertheless, the captivating properties of  $\text{o-B}_2\text{N}_2$  are poised to spur further investigations into 2D materials for the forthcoming generation of sulfur-based batteries. Notable potential advantages encompass:

- 1. Combatting Insulation:** The inherent conductivity of  $\text{o-B}_2\text{N}_2$  proficiently counters the insulation problems often associated with sulfur-based electrodes, potentially bypassing a prevalent hurdle in Li-S battery designs.
- 2. Affinity for Li-polysulfides:**  $\text{o-B}_2\text{N}_2$  displays a marked affinity for long-chain Li-polysulfides, mitigating their dissolution

into DME/DOL electrolytes, which could lead to batteries with prolonged lifespans and consistent performance.

- 3. Facilitated Redox Reactions:** The  $\text{o-B}_2\text{N}_2$  surface's propensity to preferentially attract the deposition of  $\text{Li}_2\text{S}$  catalyzes the kinetics of lithium polysulfide redox reactions, possibly contributing to faster charge and discharge rates.
- 4. Catalytic Efficiency:** Our study unravels a pioneering catalytic mechanism on the  $\text{o-B}_2\text{N}_2$  surface that significantly lowers the energy barriers for diverse sulfur reduction reactions, paving the way for increased reaction efficiency.
- 5. Shuttle Effect Mitigation:** Incorporating  $\text{o-B}_2\text{N}_2$  as a host cathode material holds immense promise in curbing the infamous shuttle effect of lithium polysulfides. This suggests batteries with better longevity and optimized performance.

Our study, while paving a novel avenue in Li-S battery material science, strongly emphasizes the unmatched potential of  $\text{o-B}_2\text{N}_2$  in revolutionizing the design of advanced Li-S batteries. Therefore, it is highly believed and hopefully, the current study can serve as a guideline for experimental discussions on the promising and versatile host cathode for Li-S battery.

#### 4. Concluding remarks

In conclusion, our study has comprehensively examined the adsorption behavior of  $\text{S}_8/\text{LiPSs}$  ( $\text{Li}_2\text{S}_n$ ,  $n = 1, 2, 4, 6,$  and  $8$ ) onto a monolayer of orthorhombic diboron dinitride ( $\text{o-B}_2\text{N}_2$ ) through systematic first-principles calculations. The investigation reveals that the  $\text{o-B}_2\text{N}_2$  monolayer exhibits characteristics of a narrow band gap semiconductor, thereby affording superior electrical conductivity relative to the h-BN monolayer. This inherent property assumes critical importance as it ensures heightened sulfur utilization and improves the kinetics of electrochemical processes. The interaction dynamics between the  $\text{o-B}_2\text{N}_2$  monolayer and LiPSs are underpinned by a synergistic dual interaction stemming from Li-B and S-B bonds. This interaction propensity



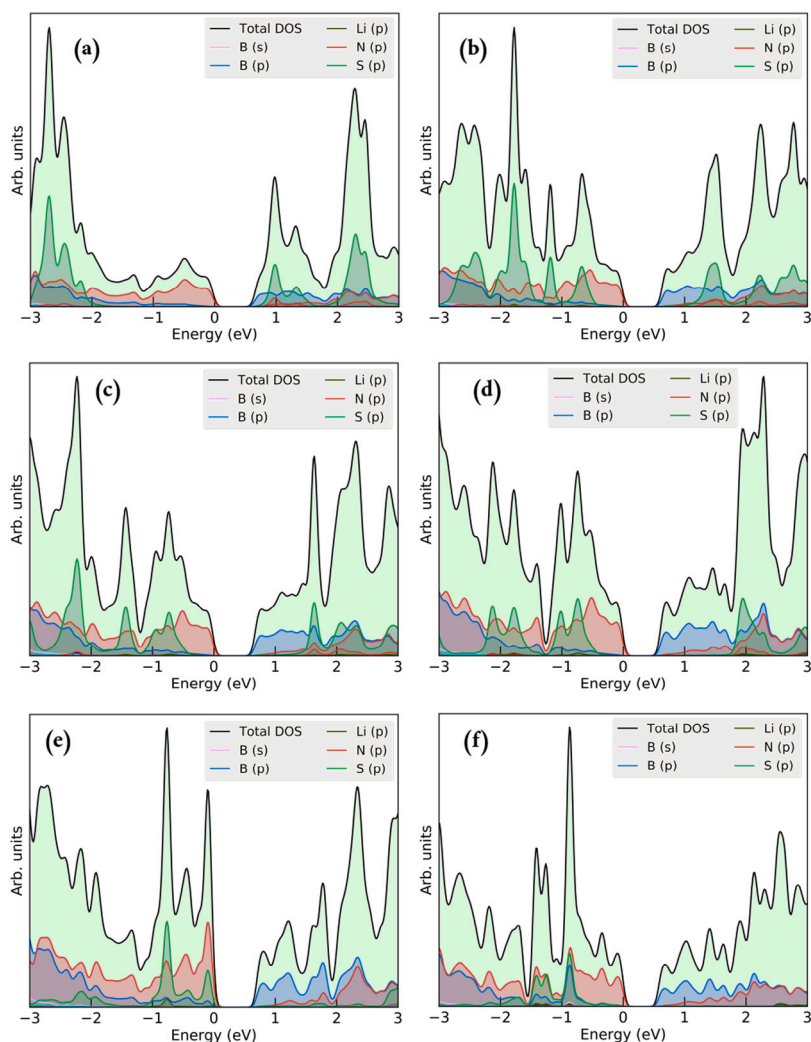


Fig. 6. Total and partial density of states projected onto different atomic orbitals of (a)  $S_8$ , (b)  $Li_2S_8$ , (c)  $Li_2S_6$ , (d)  $Li_2S_4$ , (e)  $Li_2S_2$  (f)  $Li_2S$  clusters adsorbed on  $o-B_2N_2$  surface. The Fermi level is set to zero.

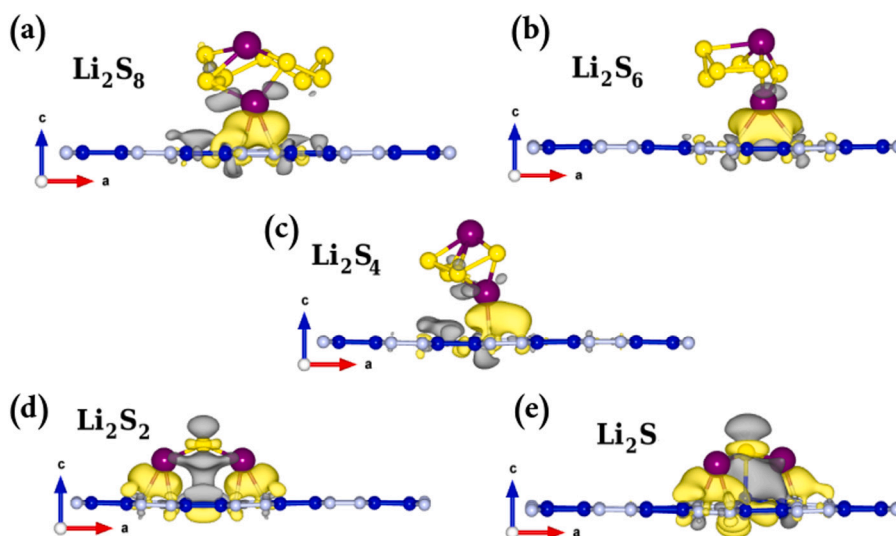


Fig. 7. Sid view of difference charge density ( $\Delta\rho$ ) for (a)  $Li_2S_8$ , (b)  $Li_2S_6$ , (c)  $Li_2S_4$ , (d)  $Li_2S_2$  (e)  $Li_2S$  clusters adsorbed on the  $o-B_2N_2$  surface, respectively. The yellow and cyan refer to electron accumulation and depletion. The isosurface is set to  $0.0015 \text{ e}\cdot\text{A}^{-3}$ . (For interpretation of the references to color in this figure legend, the reader is referred to the web version of this article.)

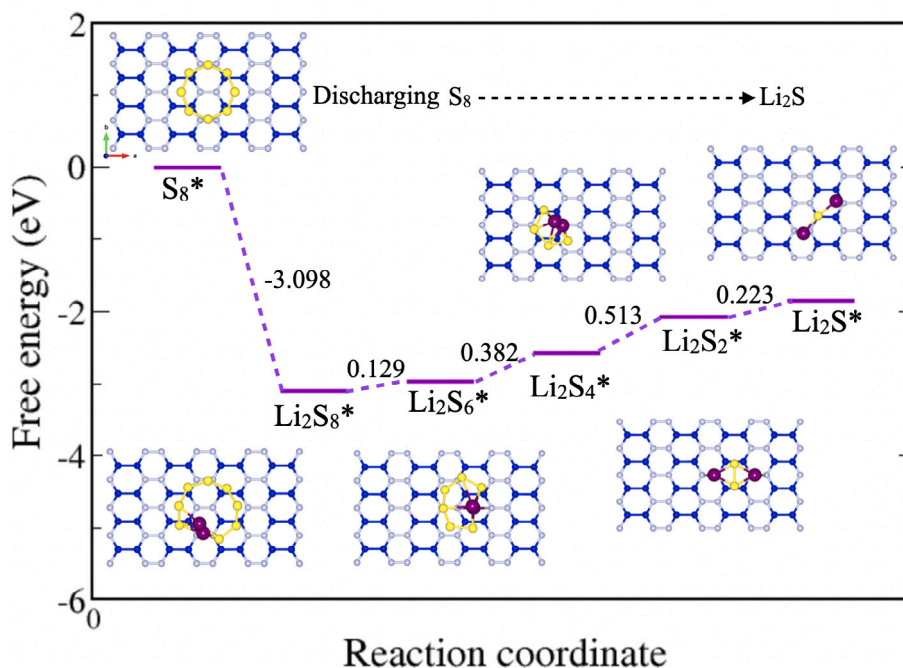


Fig. 8. Free energy profile of sulfur reduction reaction (SRR) on the 2D o-B<sub>2</sub>N<sub>2</sub> surface.

facilitates moderate interaction with LiPSs, guiding the homogeneous deposition of Li<sub>2</sub>S with uniform propagation. These findings collectively emphasize the pivotal role played by the o-B<sub>2</sub>N<sub>2</sub> monolayer in curtailing the shuttle effect of soluble LiPSs, thereby concurrently enhancing both the cycling performance and reaction rates. Notably, the investigations also uncover a low free energy barrier associated with the sulfur redox reaction (SRR) and decomposition energy barriers, thereby enhancing the catalytic mechanism of Li<sub>2</sub>S during charging and discharging processes. Given the abundant presence of both nitrogen and boron elements, this research is poised to provide a critical foundation for the advancement of optimized sulfur host materials, characterized by favorable electronic conductivity and an increased affinity for LiPSs. As such, this work holds the potential to illuminate the pathway for the future development of highly efficient and effective materials for advanced energy storage applications.

#### Declaration of competing interest

The authors declare that they have no known competing financial interests or personal relationships that could have appeared to influence the work reported in this paper.

#### Data availability

Data will be made available on request.

#### Acknowledgments

N.K. gratefully acknowledges computational resources from the Nederlandse Organisatie voor Wetenschappelijk Onderzoek (The Netherlands Organization for Scientific Research, NWO) domain Science. R.A. acknowledges the Swedish Research Council (VR-2016-06014 & VR-2020-04410), J. Gust. Richert stiftelse, Sweden (2021-00665), and SNIC (2021/1-42 and 2022/1-34) Sweden for support. A.A. acknowledges support from the PPR2 Project (MESRSF-CNRST).

#### Appendix A. Supplementary data

Supplementary material related to this article can be found online at <https://doi.org/10.1016/j.cej.2023.147518>.

#### References

- [1] X. Chen, T. Hou, K.A. Persson, Q. Zhang, Combining theory and experiment in lithium-sulfur batteries: Current progress and future perspectives, *Mater. Today* 22 (2019) 142–158.
- [2] Z.-L. Xu, S. Lin, N. Onofrio, L. Zhou, F. Shi, W. Lu, K. Kang, Q. Zhang, S.P. Lau, Exceptional catalytic effects of black phosphorus quantum dots in shuttling-free lithium sulfur batteries, *Nat. Commun.* 9 (1) (2018) 1–11.
- [3] N. Khossossi, A. Banerjee, I. Essaoudi, A. Ainane, P. Jena, R. Ahuja, Thermodynamics and kinetics of 2D g-GeC monolayer as an anode materials for Li/Na-ion batteries, *J. Power Sources* 485 (2021) 229318.
- [4] D. Singh, V. Shukla, N. Khossossi, A. Ainane, R. Ahuja, Harnessing the unique properties of mxenes for advanced rechargeable batteries, *J. Phys. Energy* 3 (1) (2020) 012005.
- [5] X.-B. Cheng, R. Zhang, C.-Z. Zhao, Q. Zhang, Toward safe lithium metal anode in rechargeable batteries: a review, *Chem. Rev.* 117 (15) (2017) 10403–10473.
- [6] S.-H. Wang, Y.-X. Yin, T.-T. Zuo, W. Dong, J.-Y. Li, J.-L. Shi, C.-H. Zhang, N.-W. Li, C.-J. Li, Y.-G. Guo, Stable Li metal anodes via regulating lithium plating/stripping in vertically aligned microchannels, *Adv. Mater.* 29 (40) (2017) 1703729.
- [7] M. Zhao, B.-Q. Li, X.-Q. Zhang, J.-Q. Huang, Q. Zhang, A perspective toward practical lithium-sulfur batteries, *ACS Cent. Sci.* 6 (7) (2020) 1095–1104.
- [8] L. Huang, J. Li, B. Liu, Y. Li, S. Shen, S. Deng, C. Lu, W. Zhang, Y. Xia, G. Pan, et al., Electrode design for lithium-sulfur batteries: problems and solutions, *Adv. Funct. Mater.* 30 (22) (2020) 1910375.
- [9] L. Fan, M. Li, X. Li, W. Xiao, Z. Chen, J. Lu, Interlayer material selection for lithium-sulfur batteries, *Joule* 3 (2) (2019) 361–386.
- [10] H. Chu, H. Noh, Y.-J. Kim, S. Yuk, J.-H. Lee, J. Lee, H. Kwack, Y. Kim, D.-K. Yang, H.-T. Kim, Achieving three-dimensional lithium sulfide growth in lithium-sulfur batteries using high-donor-number anions, *Nat. Commun.* 10 (1) (2019) 1–12.
- [11] C. Deng, Z. Wang, S. Wang, J. Yu, Inhibition of polysulfide diffusion in lithium-sulfur batteries: mechanism and improvement strategies, *J. Mater. Chem. A* 7 (20) (2019) 12381–12413.
- [12] J. Li, Y. Qu, C. Chen, X. Zhang, M. Shao, Theoretical investigation on lithium polysulfide adsorption and conversion for high-performance Li-S batteries, *Nanoscale* 13 (1) (2021) 15–35.
- [13] N. Khossossi, P.K. Panda, D. Singh, V. Shukla, Y.K. Mishra, I. Essaoudi, A. Ainane, R. Ahuja, Rational design of 2D h-BAs monolayer as advanced sulfur host for high energy density Li-S batteries, *ACS Appl. Energy Mater.* 3 (8) (2020) 7306–7317.
- [14] D. Liu, C. Zhang, G. Zhou, W. Lv, G. Ling, L. Zhi, Q.-H. Yang, Catalytic effects in lithium-sulfur batteries: promoted sulfur transformation and reduced shuttle effect, *Adv. Sci.* 5 (1) (2018) 1700270.
- [15] R. Wang, C. Luo, T. Wang, G. Zhou, Y. Deng, Y. He, Q. Zhang, F. Kang, W. Lv, Q.-H. Yang, Bidirectional catalysts for liquid-solid redox conversion in lithium-sulfur batteries, *Adv. Mater.* 32 (32) (2020) 2000315.

- [16] H. Ye, Y.-X. Yin, S. Xin, Y.-G. Guo, Tuning the porous structure of carbon hosts for loading sulfur toward long lifespan cathode materials for Li-S batteries, *J. Mater. Chem. A* 1 (22) (2013) 6602–6608.
- [17] A. Manthiram, Y. Fu, S.-H. Chung, C. Zu, Y.-S. Su, Rechargeable lithium–sulfur batteries, *Chem. Rev.* 114 (23) (2014) 11751–11787.
- [18] A. Manthiram, S.-H. Chung, C. Zu, Lithium–sulfur batteries: progress and prospects, *Adv. Mater.* 27 (12) (2015) 1980–2006.
- [19] L. Zhang, Y. Wang, Z. Niu, J. Chen, Advanced nanostructured carbon-based materials for rechargeable lithium-sulfur batteries, *Carbon* 141 (2019) 400–416.
- [20] Q. Wu, X. Zhou, J. Xu, F. Cao, C. Li, Carbon-based derivatives from metal-organic frameworks as cathode hosts for Li-S batteries, *J. Energy Chem.* 38 (2019) 94–113.
- [21] Q. Pang, X. Liang, C.Y. Kwok, L.F. Nazar, Advances in lithium–sulfur batteries based on multifunctional cathodes and electrolytes, *Nat. Energy* 1 (9) (2016) 1–11.
- [22] X. Liang, C. Hart, Q. Pang, A. Garsuch, T. Weiss, L.F. Nazar, A highly efficient polysulfide mediator for lithium–sulfur batteries, *Nat. Commun.* 6 (1) (2015) 1–8.
- [23] Z.W. Seh, W. Li, J.J. Cha, G. Zheng, Y. Yang, M.T. McDowell, P.-C. Hsu, Y. Cui, Sulphur–TiO<sub>2</sub> yolk–shell nanoarchitecture with internal void space for long-cycle lithium–sulphur batteries, *Nat. Commun.* 4 (1) (2013) 1–6.
- [24] L. Zhou, D.L. Danilov, R.-A. Eichel, P.H. Notten, Host materials anchoring polysulfides in Li-S batteries reviewed, *Adv. Energy Mater.* 11 (15) (2021) 2001304.
- [25] N.M. Abbasi, Y. Xiao, L. Zhang, L. Peng, Y. Duo, L. Wang, P. Yin, Y. Ge, H. Zhu, B. Zhang, et al., Heterostructures of titanium-based mxene in energy conversion and storage devices, *J. Mater. Chem. C* (2021).
- [26] Y. Li, D. Ye, W. Liu, B. Shi, R. Guo, H. Zhao, H. Pei, J. Xu, J. Xie, A MnO<sub>2</sub>/graphene oxide/multi-walled carbon nanotubes-sulfur composite with dual-efficient polysulfide adsorption for improving lithium-sulfur batteries, *ACS Appl. Mater. Interfaces* 8 (42) (2016) 28566–28573.
- [27] X. Yu, X. Zhu, Z. Pei, Y. Li, C. Li, Z. Sui, Nitrogen-doped porous graphene/MnO<sub>2</sub> composite as sulfur hosts for lithium-sulfur batteries, *Diam. Relat. Mater.* (2021) 108497.
- [28] Y. Liu, Y. Zhang, Y. Liu, J. Zhu, Z. Ge, Z. Li, Y. Chen, Super heating/cooling rate enabled by microwave shock on polymeric graphene foam for high performance lithium–sulfur batteries, *Carbon* 173 (2021) 809–816.
- [29] H. Li, L. Sun, Y. Zhang, T. Tan, G. Wang, Z. Bakonov, Enhanced cycle performance of Li/S battery with the reduced graphene oxide/activated carbon functional interlayer, *J. Energy Chem.* 26 (6) (2017) 1276–1281.
- [30] G.D. Park, J. Lee, Y. Piao, Y.C. Kang, Mesoporous graphitic carbon-TiO<sub>2</sub> composite microspheres produced by a pilot-scale spray-drying process as an efficient sulfur host material for Li-S batteries, *Chem. Eng. J.* 335 (2018) 600–611.
- [31] Q. Shao, Z.-S. Wu, J. Chen, Two-dimensional materials for advanced Li-S batteries, *Energy Storage Mater.* 22 (2019) 284–310.
- [32] K. Sun, M. Fu, Z. Xie, D. Su, H. Zhong, J. Bai, E. Dooryhee, H. Gan, Improvement of Li-S battery electrochemical performance with 2D TiS<sub>2</sub> additive, *Electrochim. Acta* 292 (2018) 779–788.
- [33] L. Zhang, P. Liang, H.-b. Shu, X.-l. Man, F. Li, J. Huang, Q.-m. Dong, D.-l. Chao, Borophene as efficient sulfur hosts for lithium–sulfur batteries: suppressing shuttle effect and improving conductivity, *J. Phys. Chem. C* 121 (29) (2017) 15549–15555.
- [34] S. Mukherjee, L. Kavalsky, K. Chattopadhyay, C.V. Singh, Adsorption and diffusion of lithium polysulfides over blue phosphorene for Li-S batteries, *Nanoscale* 10 (45) (2018) 21335–21352.
- [35] L. Li, L. Chen, S. Mukherjee, J. Gao, H. Sun, Z. Liu, X. Ma, T. Gupta, C.V. Singh, W. Ren, et al., Phosphorene as a polysulfide immobilizer and catalyst in high-performance lithium–sulfur batteries, *Adv. Mater.* 29 (2) (2017) 1602734.
- [36] J. Zhao, Y. Yang, R.S. Katiyar, Z. Chen, Phosphorene as a promising anchoring material for lithium–sulfur batteries: a computational study, *J. Mater. Chem. A* 4 (16) (2016) 6124–6130.
- [37] Y. Zheng, H. Li, H. Yuan, H. Fan, W. Li, J. Zhang, Understanding the anchoring effect of graphene, BN, C<sub>2</sub>N and C<sub>3</sub>N<sub>4</sub> monolayers for lithium– polysulfides in Li-S batteries, *Appl. Surf. Sci.* 434 (2018) 596–603.
- [38] D.R. Deng, F. Xue, C.-D. Bai, J. Lei, R. Yuan, M.S. Zheng, Q.F. Dong, Enhanced adsorptions to polysulfides on graphene-supported BN nanosheets with excellent Li-S battery performance in a wide temperature range, *ACS Nano* 12 (11) (2018) 11120–11129.
- [39] H. Al Salem, V.R. Chitturi, G. Babu, J.A. Santana, D. Gopalakrishnan, L.M.R. Arava, Stabilizing polysulfide-shuttle in a Li-S battery using transition metal carbide nanostructures, *RSC Adv.* 6 (111) (2016) 110301–110306.
- [40] N. Mosavati, S.O. Salley, K.S. Ng, Characterization and electrochemical activities of nanostructured transition metal nitrides as cathode materials for lithium sulfur batteries, *J. Power Sources* 340 (2017) 210–216.
- [41] G. Babu, N. Masurkar, H. Al Salem, L.M.R. Arava, Transition metal dichalcogenide atomic layers for lithium polysulfides electrocatalysis, *J. Am. Chem. Soc.* 139 (1) (2017) 171–178.
- [42] X. Liang, C.Y. Kwok, F. Lodi-Marzano, Q. Pang, M. Cuisinier, H. Huang, C.J. Hart, D. Houtarde, K. Kaup, H. Sommer, et al., Tuning transition metal oxide–sulfur interactions for long life lithium sulfur batteries: the “Goldilocks” principle, *Adv. Energy Mater.* 6 (6) (2016) 1501636.
- [43] K. Mahankali, N.K. Thangavel, D. Gopchenko, L.M.R. Arava, Atomically engineered transition metal dichalcogenides for liquid polysulfide adsorption and their effective conversion in Li-S batteries, *ACS Appl. Mater. Interfaces* 12 (24) (2020) 27112–27121.
- [44] K. Watanabe, T. Taniguchi, H. Kanda, Direct-bandgap properties and evidence for ultraviolet lasing of hexagonal boron nitride single crystal, *Nat. Mater.* 3 (6) (2004) 404–409.
- [45] Y. Kubota, K. Watanabe, O. Tsuda, T. Taniguchi, Deep ultraviolet light-emitting hexagonal boron nitride synthesized at atmospheric pressure, *Science* 317 (5840) (2007) 932–934.
- [46] X. Liang, Y. Rangom, C.Y. Kwok, Q. Pang, L.F. Nazar, Interwoven MXene nanosheet/carbon-nanotube composites as Li-S cathode hosts, *Adv. Mater.* 29 (3) (2017) 1603040.
- [47] Q. Pang, D. Kundu, L.F. Nazar, A graphene-like metallic cathode host for long-life and high-loading lithium–sulfur batteries, *Mater. Horiz.* 3 (2) (2016) 130–136.
- [48] S. Demirci, S.E. Rad, S. Kazak, S. Nezir, S. Jahangirov, Monolayer diboron dinitride: Direct band-gap semiconductor with high absorption in the visible range, *Phys. Rev. B* 101 (12) (2020) 125408.
- [49] G. Kresse, J. Furthmüller, Efficient iterative schemes for ab initio total-energy calculations using a plane-wave basis set, *Phys. Rev. B* 54 (16) (1996) 11169.
- [50] J.P. Perdew, K. Burke, M. Ernzerhof, Generalized gradient approximation made simple, *Phys. Rev. Lett.* 77 (18) (1996) 3865.
- [51] H.J. Monkhorst, J.D. Pack, Special points for Brillouin-zone integrations, *Phys. Rev. B* 13 (12) (1976) 5188.
- [52] G. Henkelman, A. Arnaldsson, H. Jónsson, A fast and robust algorithm for Bader decomposition of charge density, *Comput. Mater. Sci.* 36 (3) (2006) 354–360.
- [53] L. Peng, Z. Wei, C. Wan, J. Li, Z. Chen, D. Zhu, D. Baumann, H. Liu, C.S. Allen, X. Xu, et al., A fundamental look at electrocatalytic sulfur reduction reaction, *Nat. Catal.* 3 (9) (2020) 762–770.
- [54] Z. Du, X. Chen, W. Hu, C. Chuang, S. Xie, A. Hu, W. Yan, X. Kong, X. Wu, H. Ji, et al., Cobalt in nitrogen-doped graphene as single-atom catalyst for high-sulfur content lithium–sulfur batteries, *J. Am. Chem. Soc.* 141 (9) (2019) 3977–3985.
- [55] X. Song, Y. Qu, L. Zhao, M. Zhao, Monolayer Fe<sub>3</sub>GeX<sub>2</sub> (X=S, Se, and Te) as highly efficient electrocatalysts for lithium–sulfur batteries, *ACS Appl. Mater. Interfaces* 13 (10) (2021) 11845–11851.
- [56] J. Zhao, H. Zeng, G. Yao, Computational design of a polymorph for 2D III–V orthorhombic monolayers by first principles calculations: excellent anisotropic, electronic and optical properties, *Phys. Chem. Chem. Phys.* 23 (6) (2021) 3771–3778.
- [57] M. Fang, X. Liu, J.-C. Ren, S. Yang, G. Su, Q. Fang, J. Lai, S. Li, W. Liu, Revisiting the anchoring behavior in lithium-sulfur batteries: many-body effect on the suppression of shuttle effect, *npj Comput. Mater.* 6 (1) (2020) 1–6.
- [58] T.-Z. Hou, W.-T. Xu, X. Chen, H.-J. Peng, J.-Q. Huang, Q. Zhang, Lithium bond chemistry in lithium–sulfur batteries, *Angew. Chem.* 129 (28) (2017) 8290–8294.
- [59] T. Maihom, S. Kaewruang, N. Phattharasupakun, P. Chiochan, J. Limtrakul, M. Sawangphruk, Lithium bond impact on lithium polysulfide adsorption with functionalized carbon fiber paper interlayers for lithium–sulfur batteries, *J. Phys. Chem. C* 122 (13) (2018) 7033–7040.
- [60] X. Chen, H.-J. Peng, R. Zhang, T.-Z. Hou, J.-Q. Huang, B. Li, Q. Zhang, An analogous periodic law for strong anchoring of polysulfides on polar hosts in lithium sulfur batteries: S- or Li-binding on first-row transition-metal sulfides? *ACS Energy Lett.* 2 (4) (2017) 795–801.
- [61] Q. Zhang, Y. Wang, Z.W. Seh, Z. Fu, R. Zhang, Y. Cui, Understanding the anchoring effect of two-dimensional layered materials for lithium–sulfur batteries, *Nano Lett.* 15 (6) (2015) 3780–3786.
- [62] F.Y. Fan, W.H. Woodford, Z. Li, N. Baram, K.C. Smith, A. Helal, G.H. McKinley, W.C. Carter, Y.-M. Chiang, Polysulfide flow batteries enabled by percolating nanoscale conductor networks, *Nano Lett.* 14 (4) (2014) 2210–2218.
- [63] Z.W. Seh, Y. Sun, Q. Zhang, Y. Cui, Designing high-energy lithium–sulfur batteries, *Chem. Soc. Rev.* 45 (20) (2016) 5605–5634.
- [64] K. Sun, Q. Wu, X. Tong, H. Gan, Electrolyte with low polysulfide solubility for Li-S batteries, *ACS Appl. Energy Mater.* 1 (6) (2018) 2608–2618.
- [65] L. Kong, X. Chen, B.-Q. Li, H.-J. Peng, J.-Q. Huang, J. Xie, Q. Zhang, A bifunctional perovskite promoter for polysulfide regulation toward stable lithium–sulfur batteries, *Adv. Mater.* 30 (2) (2018) 1705219.
- [66] G. Henkelman, H. Jónsson, Improved tangent estimate in the nudged elastic band method for finding minimum energy paths and saddle points, *J. Chem. Phys.* 113 (22) (2000) 9978–9985.
- [67] G. Henkelman, B.P. Uberuaga, H. Jónsson, A climbing image nudged elastic band method for finding saddle points and minimum energy paths, *J. Chem. Phys.* 113 (22) (2000) 9901–9904.
- [68] G. Zhou, H. Tian, Y. Jin, X. Tao, B. Liu, R. Zhang, Z.W. Seh, D. Zhuo, Y. Liu, J. Sun, et al., Catalytic oxidation of Li<sub>2</sub>S on the surface of metal sulfides for Li-S batteries, *Proc. Natl. Acad. Sci.* 114 (5) (2017) 840–845.
- [69] R.S. Assary, L.A. Curtiss, J.S. Moore, Toward a molecular understanding of energetics in Li-S batteries using nonaqueous electrolytes: a high-level quantum chemical study, *J. Phys. Chem. C* 118 (2024) 11545–11558.
- [70] G. Zhou, S. Zhao, T. Wang, S.-Z. Yang, B. Johannessen, H. Chen, C. Liu, Y. Ye, Y. Wu, Y. Peng, et al., Theoretical calculation guided design of single-atom catalysts toward fast kinetic and long-life Li-S batteries, *Nano Lett.* 20 (2) (2019) 1252–1261.